

Quantification of arterial flow using digital subtraction angiography

Odile Bonnefous

Philips Research, Paris 92150, France

Vitor Mendes Pereira, Rafik Ouared, and Olivier Brina

Department of Medical Imaging and Information Sciences, Interventional Neuroradiology Unit, University Hospitals of Geneva, Geneva 1211, Switzerland

Hans Aerts, Roel Hermans, Fred van Nijnatten, Jean Stawiaski, and Daniel Ruijters^{a)}

Interventional X-Ray, Philips Healthcare, Best 5680DA, The Netherlands

(Received 29 March 2012; revised 31 August 2012; accepted for publication 1 September 2012; published 27 September 2012)

Purpose: In this paper, a method for the estimation of arterial hemodynamic flow from x-ray video densitometry data is proposed and validated using an *in vitro* setup.

Methods: The method is based on the acquisition of three-dimensional rotational angiography and digital subtraction angiography sequences. A modest contrast injection rate (between 1 and 4 ml/s) leads to a contrast density that is modulated by the cardiac cycle, which can be measured in the x-ray signal. An optical flow based approach is used to estimate the blood flow velocities from the cyclic phases in the x-ray signal.

Results: The authors have validated this method *in vitro*, and present three clinical cases. The *in vitro* experiments compared the x-ray video densitometry results with the gold standard delivered by a flow meter. Linear correlation analysis and regression fitting showed that the ideal slope of 1 and intercept of 0 were contained within the 95 percentile confidence interval. The results show that a frame rate higher than 50 Hz allows measuring flows in the range of 2 ml/s to 6 ml/s within an accuracy of 5%.

Conclusions: The *in vitro* and clinical results indicate that it is feasible to estimate blood flow in routine interventional procedures. The availability of an x-ray based method for quantitative flow estimation is particularly clinically useful for intra-cranial applications, where other methods, such as ultrasound Doppler, are not available. © 2012 American Association of Physicists in Medicine. [<http://dx.doi.org/10.1118/1.4754299>]

Key words: arterial flow, digital subtraction angiography, video densitometry

I. INTRODUCTION

In the domain of interventional x-ray imaging, digital subtraction angiography (DSA) and three-dimensional rotational angiography (3DRA) are the gold standard for imaging vascular lesions. Though these provide valuable information regarding the vascular morphology, it is still difficult to extract functional information from DSA. The recent advancements in minimal invasive treatment of vascular lesions, however, could considerably benefit from the availability of quantitative functional measurements during the course of the interventional procedure. For example, the flow pattern inside aneurysms is considered to be one of the parameters that can be used to predict rupture and clotting.^{1,2} Also in stenosis grading, arterio-venous malformations, and post-interventional hyperperfusion flow measurements can be valuable.³⁻⁶

In this paper, a radiological technique for the quantitative assessment of a functional parameter, hemodynamic flow, is examined. Quantitatively measuring the blood flow by using x-ray video densitometry, based on the detection of the displacement of radio-opaque contrast material through the vascular system, has been studied since the 1960s. Shpilfoygel *et al.*⁷ provided a review of the literature in 2000, and divided the cited methods into two main classes: tracking and compu-

tational methods. Since 2000, several new publications on this topic have appeared. Sarry *et al.*⁸ estimate the flow using an inverse advection model. Bogunovic and Loncaric⁹ proposed the combination of 2D DSA and 3DRA, using an analysis of the time density curves. Rhode *et al.*¹⁰ described a combination of a model based and an optical flow approach. Waechter *et al.*¹¹ proposed a model based approach using a 3DRA acquisition. Many methods consider the pulsatile character of blood flow as a hurdle that has to be overcome, whereas we use only the modulation by the cardiac cycle to extract the flow velocities.

The technique described in this paper is based on the acquisition of 2D DSA sequences, in combination with a 3DRA acquisition. This technique measures the flow values from the angiographic DSA sequence, which are acquired using a dedicated injection protocol. It exploits the transportation of contrast fluid injected into the arterial blood stream. Due to the pulsatile character of the blood flow, contrast patterns are created that propagate in the vascular network. Using image processing techniques, velocity profiles are obtained from the motion of these patterns. Finally the profiles are converted to flow values. The algorithm does not rely on prior knowledge of flow models or injection curves, contrary to the previously cited publications. To explore the validity of this approach, we tested it using vascular phantoms. In an *in vitro* setup we

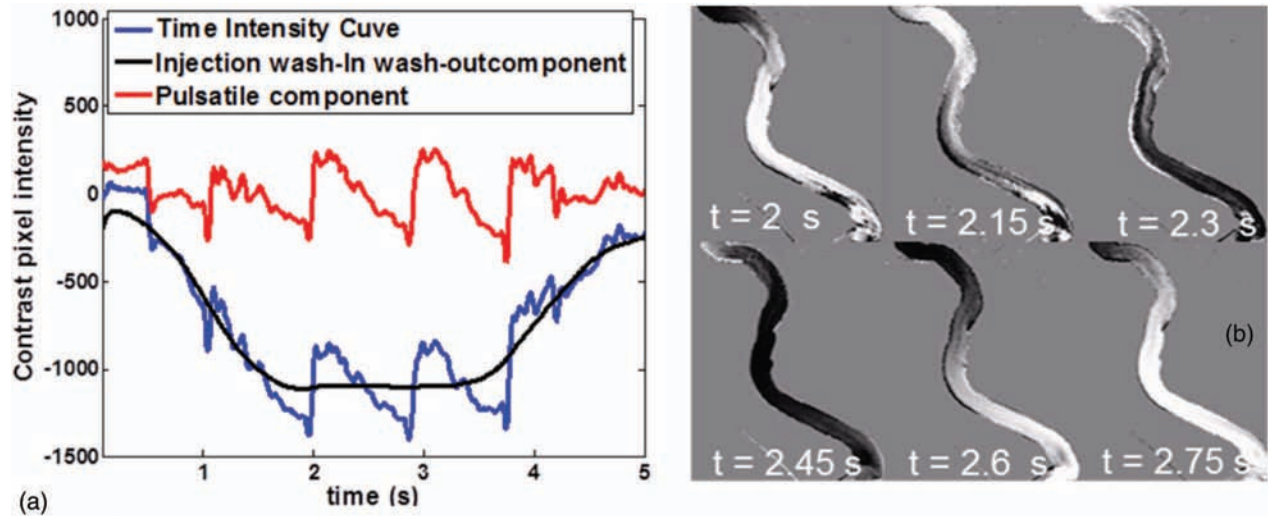


FIG. 1. (a) Time intensity curve (bottom modulated curve), decomposed into the wash-in/wash-out component (bottom smooth curve), and the contrast wave component (top curve). (b) Propagation of the contrast wave.

compared x-ray based flow estimations to values recorded by flow meters. Furthermore, we explored various injection protocols in order to determine the appropriate injection parameters. In addition, we evaluated it on several clinical cases acquired during interventional procedures by comparing Doppler ultrasound flow measurements with x-ray based flow measurements.

II. MATERIALS AND METHODS

II.A. Principles

Our approach is based on following the contrast density in the vessels modulated by the cardiac phase. When injecting contrast into an artery, blood and contrast medium mix proportionally to their respective flow rates. Therefore, during systole the dilution of the contrast medium entering the artery is higher than during diastole. The physiological pulsatility of the blood flow therefore adds a periodic modulation on top of a regular dilution of contrast [Fig. 1(a)]. The low frequent regular dilution is subtracted from the x-ray signal, in order to process only the periodic modulation. Downstream the injection point, this modulation is transported through the vessels by the flow [Fig. 1(b)].

The 3D vessel axis $\vec{a}(z)$ and the cross-section $S(z)$ of the artery are extracted from the 3DRA volume [Fig. 2(a)], whereby z denotes the distance along the vessel centerline. The 3D arterial axis is projected on the 2D acquisition plane [Fig. 2(b)], the vessel image is bent along the straight vascular axis and the foreshortening is corrected. The contrast data in the 2D acquisition are integrated over the cross-section of the artery. This forms the contrast wave map $C(t, z)$ [Fig. 2(c)], which displays the progression of the contrast wave along the vascular axis. The velocity displacement of the periodically modulated contrast wave is followed using an optical flow algorithm similar to Refs. 10, 12, and 13. This method calculates the motion dz of a contrast sample $C(t, z)$, $C(t + dt, z + dz)$ which is taken at times t and $t + dt$, under the as-

sumption that the diffusion of contrast medium into blood is negligible. The corresponding equation is

$$\frac{\partial C}{\partial t} + \frac{\partial C}{\partial z} V(t, z) = 0, \quad (1)$$

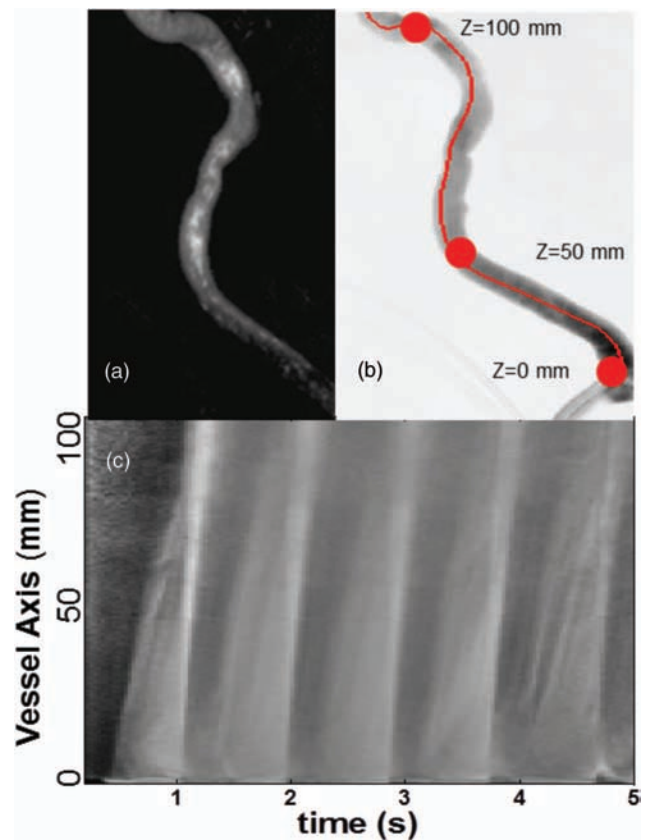


FIG. 2. Construction of the contrast wave map. The wave map describes how the contrast pattern is distributed along the arterial axis at a given time index, and is used to determine the motion of the contrast using the optical flow principle. (a) 3DRA. (b) Projection of 3D vessel axis on 2D image. (c) Contrast wave map. The contrast wave map contain the DSA intensities along the projected centerline over time.

whereby $V(t, z)$ is the displacement velocity and is calculated by using an adaptive least square resolution method.^{14,15} Hereby, the quadratic error is given as

$$E^2 = \left(\frac{\partial C}{\partial t} + \frac{\partial C}{\partial z} V(t, z) \right)^2. \quad (2)$$

The least square solution is obtained by the formula

$$\hat{V}(t, z) = \left\langle -\frac{\partial C}{\partial t} \cdot \frac{\partial C}{\partial z} \right\rangle / \left\langle \left(\frac{\partial C}{\partial z} \right)^2 \right\rangle, \quad (3)$$

where $\langle \cdot \rangle$ stands for spatial averaging over a given window, and \hat{V} is the resulting estimated velocity. This simple resolution is only adequate for small displacements. To cope with larger velocities, we use an iterative warping process¹⁶ to model the displacement of the contrast wave between two consecutive frames, which is defined as

$$\tilde{C}_k(t, z) = \tilde{C}_{k-1}(t, z - \Delta t \cdot \hat{V}_{k-1}(t, z)), \quad (4)$$

whereby \tilde{C}_k represents the warped contrast wave after k iterations, \hat{V}_k the velocity contribution calculated in this iteration, and Δt being the time between two consecutive frames. The iterative process is initialized with $\tilde{C}_0(t, z) = C(t, z)$. The temporal derivative $\partial C / \partial t$ is then approximated by

$$\frac{\tilde{C}_k(t, z) - C(t - \Delta t, z)}{\Delta t}, \quad (5)$$

and filled in Eqs. (2) and (3). The iterative process stops when the quadratic error does not decrease anymore. The remaining error is used to validate the measured velocity. The overall velocity is the calculated as

$$V(t, z) = \sum_k \hat{V}_k(t, z). \quad (6)$$

Using the section profile extracted from the 3DRA volume, the volume flow curve is averaged along the arterial segment length L with

$$Q(t) = \frac{1}{L} \int S(z) V(t, z) dz. \quad (7)$$

$Q(t)$ comprises the contributions of the blood flow, as well as the contrast injection volume.

II.B. Materials

II.B.1. Vascular phantoms

We performed tests using controlled flow phantom experiments. A continuous pump, modulated by a pulsatile system created conditions similar to arterial flows (Figs. 3 and 4). An electromagnetic flow meter was installed in the circulatory system to record the instantaneous flow values. As vascular phantoms, we used two different phantoms: the first phantom concerned a simple straight 4 mm diameter tube, and the second phantom was shaped based on a 3D acquisition of a cerebral vessel with an average diameter of 5 mm (min = 4.8 mm, max = 5.3 mm). For both phantoms, the distance from the contrast injection to the measurement area was larger than 10 cm, in order to achieve a sufficient mix of the contrast medium and the fluid.¹⁷

Using the straight phantom, 19 x-ray sequences were acquired and based upon those sequences the flow was determined in 247 conditions using various settings. We varied the following parameters:

- The steady flow pump rate: [0.83, 1.66, 2.5, 3.33] ml/s.
- The modulating pulsatile flow pump: amplitude: [0.3, 0.5, 0.7, 0.9, 1.1] ml/s, frequency: 1.2 Hz.

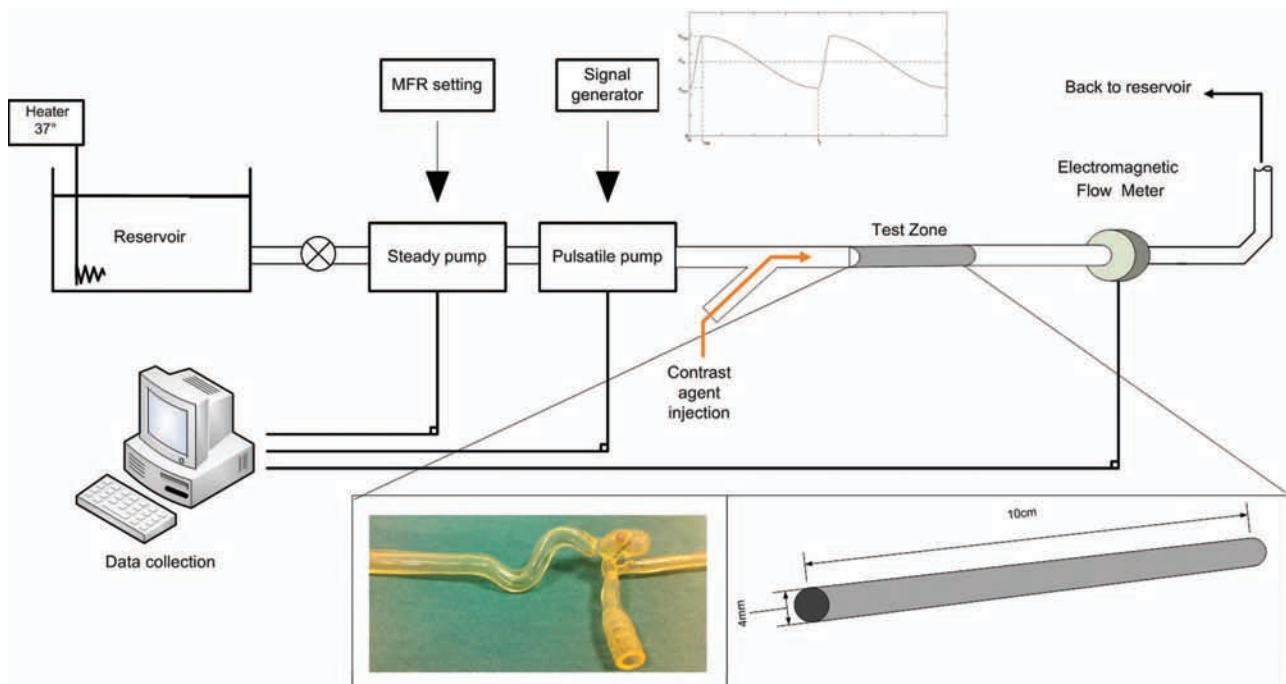


FIG. 3. Experimental setup comprising a steady pump, a pulsatile pump, an electromagnetic flow meter, and the circulating circuit. Both phantoms were used in this setup.

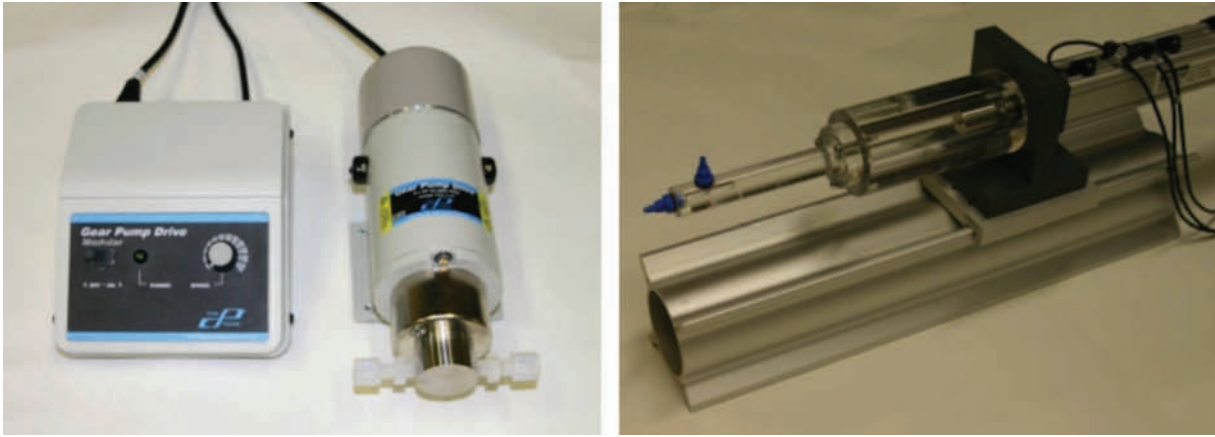


FIG. 4. Steady pump (left) and pulsatile pump (right).

- The contrast injection: rate: [1, 2, 3, 4] ml/s, duration: [1, 2, 3, 4] s.
- The acquisition frame rate: [150 (original) and 75, 50, 30, 25, 15 (under sampled)] Hz.
- The added noise level, signal to noise ratio SNR: [10, 20, 6] dB.
- The arterial segment length used for measurement: [10, 20, 30, 40, 50] mm.

Some of those parameters were varied artificially: the noise level by adding noise to the data, the acquisition frame rate by under-sampling the acquired sequences and the arterial segment length by considering a region of interest (ROI) cut in the x-ray images. The *in vitro* experiments with the straight phantom were conducted using a modified flat panel x-ray system, which could read out im-

ages at a maximal frame rate of 150 frames per second. The x-ray images were acquired using a field of view of 800×800 pixels, using 3×3 binned pixels of $150 \mu\text{m}^2$. The source-to-detector distance was 102 cm and the source-to-object distance 82 cm. The x-ray tube current settings were about 75 kV and 550 mAs, yielding a dose of 222 nGy per frame. Perspex (6.1 cm) was used as scatter material.

With the cerebral vessel phantom 22 x-ray sequences were recorded, while the same phantom region was used for measurements, see Fig. 5. The arterial segment length used for the measurements was 30 mm. The following parameters were varied in the experiment:

- Two different viewing angles on the phantom were used.

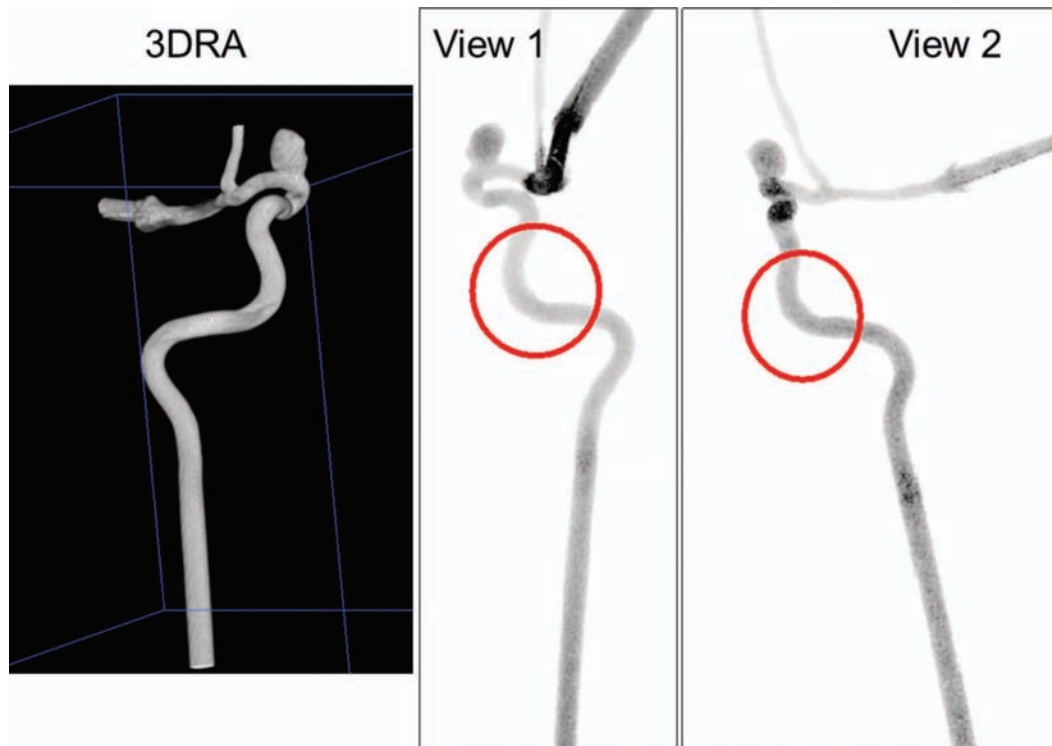


FIG. 5. 3DRA reconstruction of the cerebral vessel phantom (left), and the two views that were used for measurements (middle and right).

- The steady flow pump rate: [1, 2, 3, 4] ml/s.
- The modulating pulsatile flow pump amplitude: [40%, 70%, 100%] of the steady flow rate.
- The modulating pulsatile flow pump frequency: [1, 1.3] Hz.
- The contrast injection: rate: [1, 1.5, 2, 3] ml/s.

The injection duration was 4 s for all experiments with this phantom, and all x-ray sequences were recorded at a frame rate of 60 frames per second, using a regular flat panel detector (Allura FD20, Philips Healthcare, Best, the Netherlands). The field of view consisted of 234 by 432 pixels with a 2×2 binned pixel size of $308 \mu\text{m}^2$. The source-to-detector distance was 118 cm and the source-to-object distance 81 cm. The nominal x-ray acquisition settings were 70 kV and 630 mAs, and the dose was set to 64 nGy per frame.

II.B.2. Clinical cases

The three presented patients had been admitted to receive endovascular treatment of an unruptured cerebral aneurysm, following the institutional ethics committee's approval of a protocol submitted for epidemiology and hemodynamic investigations on IAs (NEC 07-056). To test the clinical utilization of the technique, the flow was measured in the carotid artery using the technique described in this paper and with Doppler ultrasound as gold standard. To this purpose, Doppler ultrasound measurements were acquired before the x-ray flow measurements, but as close as possible in time. They were performed by an experienced neurologist to ensure repeatability of the measurements. The measurement was performed on the internal carotid artery with a submandibular approach. The arterial cross-section used for Doppler ultrasound measurements was located within the vessel segment used for the angiographic measurements. Peri-interventionally, a 3DRA volume and several angiographic 2D sequences characterized by their injection rates (1.5 cc/s, 2 cc/s, 3 cc/s) and duration (3 s) were acquired for a selected region of interest in the carotid

artery. The different injection rates are used to cover the large variation of the patient's mean flow rate in order to be sure to get pulsatile information in patients since the mean flow rate is unknown when the DSA is being acquired. From a femoral approach, a 5F/0.038 inch catheter (Cook, Inc.) was placed in the internal carotid artery, 3 cm distal to the carotid artery bifurcation. A straight arterial segment with a length of at least 20 mm was used for the measurements. The frame rate of the x-ray system was set to 60 frames/s. The angiographic exams were acquired with an angiographic C-arm system (Allura FD20, Philips Healthcare, Best, the Netherlands). The Womersley model¹⁸ was used to create the reference volume flow curve out of the Doppler trace and the artery diameter (Fig. 6).

II.C. Analysis methods

The gold standard data and x-ray mean flow values are compared using linear correlation analysis for the phantom experiments and the clinical data. The electromagnetic flow meter measurements served as gold standard for the phantom experiments, and the Doppler ultrasound for the patient measurements. In order to analyze the results, the flow $Q(t)$ is averaged over the duration of one cardiac period T , delivering the mean flow $\hat{Q}(t)$:

$$\hat{Q}(t) = \frac{1}{T} \int_{t-T/2}^{t+T/2} Q(u) du. \quad (8)$$

From the mean flow sequence the maximum value is determined:

$$Q_0 = \max[\hat{Q}(t)]. \quad (9)$$

Subscripts X and R are being used to denote the x-ray and gold standard reference data, respectively. Linear correlation analysis and regression fitting are used to compare Q_{X0} and Q_{R0} , whereby a line is fitted through the x-ray and gold standard data pairs, using a least square fit. The slope and intercept of the fitted line are then examined, which are in the ideal case 1

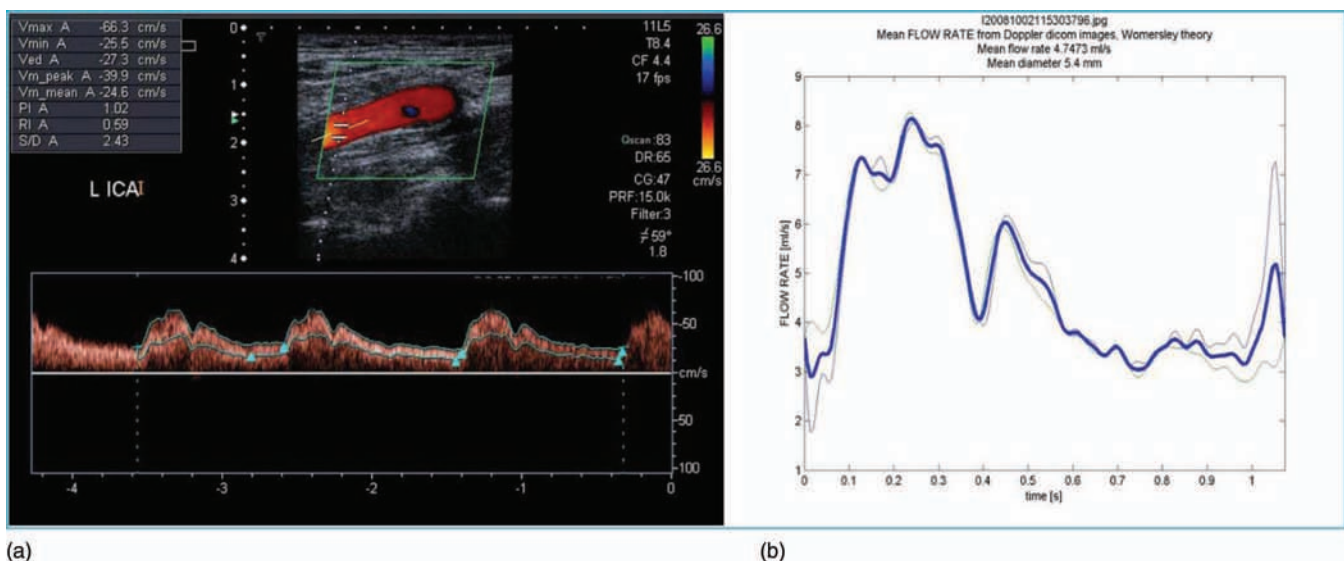


FIG. 6. Volume flow estimation using Doppler recordings. (a) Doppler trace and maximum velocity curve. (b) Volume flow curve using the Womersley model.

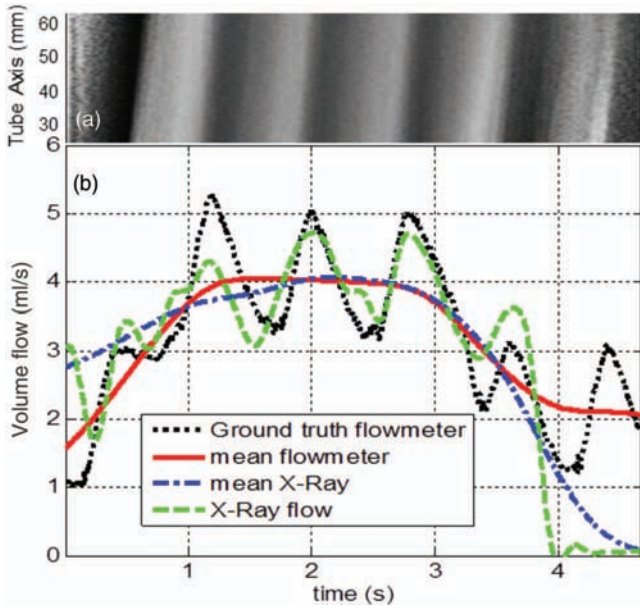


FIG. 7. Flow phantom experiment: (a) Contrast wave map as a function of time (x) and position along the arterial axis (y). Darker intensities correspond to lower contrast medium densities. (b) Flow curves from flow meter and x-ray technique, aligned with the contrast wave map. When injecting contrast into an artery, blood and contrast medium mix proportionally to their respective flow rates. Therefore, high blood flow values lead to lower contrast medium concentrations (darker), and vice versa.

and 0, respectively. For each fitted line the coefficient of determination R^2 , and for the slope and intercept the standard error and the 95 percentile confidence interval (95% CI), are determined.

III. RESULTS

III.A. Phantoms

Figure 7 shows the experimental contrast wave map for a particular acquisition [Fig. 7(a)] and the corresponding flow curves [Fig. 7(b)]. The reference curves $Q_R(t)$ (ground truth

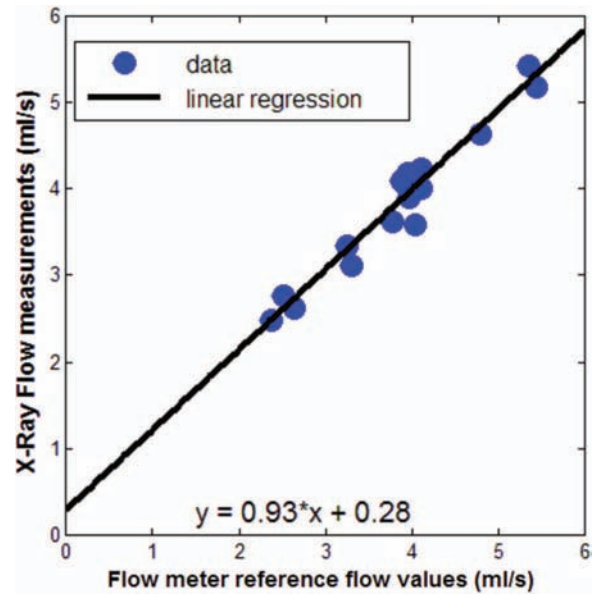


FIG. 8. X-ray and flow meter measurement fitting for $fr = 50$ Hz, $L = 30$ mm.

flow meter) and $\hat{Q}_R(t)$ (mean flow meter) and the x-ray curves $Q_X(t)$ (x-ray flow) and $\hat{Q}_X(t)$ (mean x-ray flow) are superimposed. Table I presents the complete overview of the maxima of all measured curves with the straight phantom. Table II provides the statistical analysis of the measurements in Table I, whereby either the frame rate fr , the vessel segment length L , or the signal to noise ratio SNR are varied, while the other parameters are kept constant. This table contains the linear fitting results, comparing the reference and x-ray flow measurements (Q_{R0} and Q_{X0}). The determination coefficients R^2 of the fit are listed, the slopes and the intercepts, as well as the corresponding standard errors with their 95% CIs. These evaluations have been obtained with a significance level $p < 0.0001$. An example of the fitting between the flow meter reference and x-ray measurement is shown in Fig. 8 for $fr = 50$ Hz, $L = 30$ mm, no noise added.

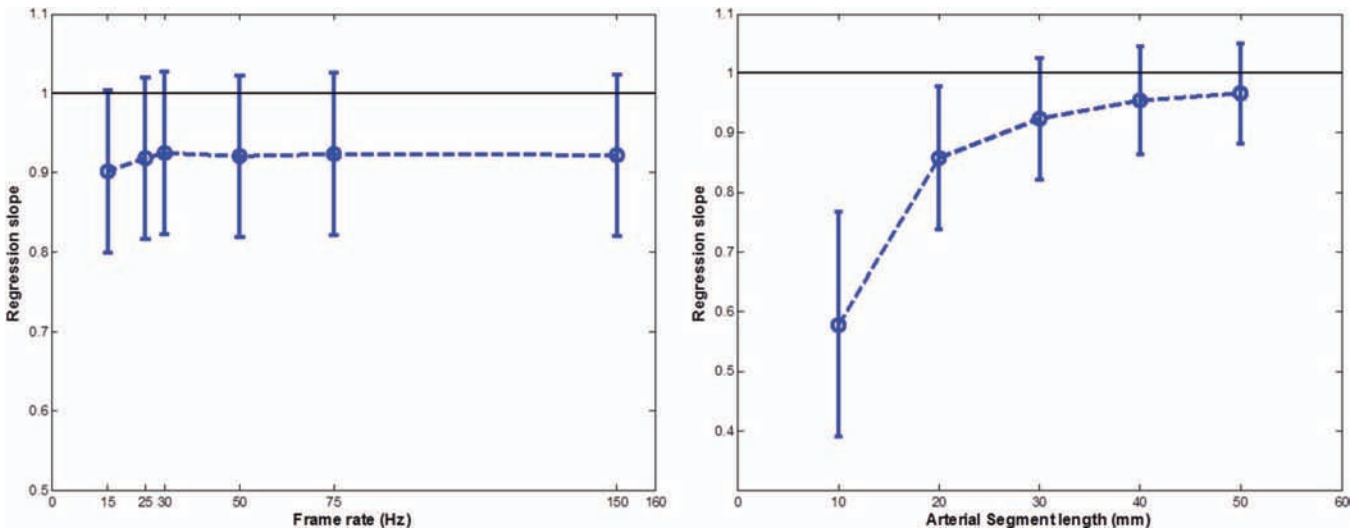


FIG. 9. Regression slope coefficients with 95% CIs obtained regression of x-ray flow measurements on reference flow meter values. Left: Slopes varying with the frame rate for a fixed vessel length of 30 mm. Right: Slopes varying with the vessel length for a fixed frame rate of 50 Hz.

TABLE I. Experimental conditions and flow estimations during *in vitro* experiments on the straight phantom.

	Injection			X-ray													
	Rate (ml/s)	Time (s)	Flow meter (ml/s)	fr = 150 Hz,	fr = 75 Hz,	fr = 50 Hz,	fr = 30 Hz,	fr = 25 Hz,	fr = 15 Hz,	fr = 50 Hz,	fr = 50 Hz,	fr = 50 Hz,					
				L = 30 mm	L = 30 mm	L = 30 mm	L = 30 mm	L = 30 mm	L = 30 mm	L = 30 mm	L = 10 mm	L = 20 mm	L = 40 mm	L = 50 mm	L = 30 mm, n = 6 dB	L = 30 mm, n = 10 dB	L = 30 mm, n = 20 dB
Expt. 1	3	2	4.07	3.63	3.63	3.62	3.58	3.57	3.43	2.50	3.44	3.72	3.79	2.99	3.31	3.61	
Expt. 2	3	2	4.11	4.03	4.03	4.02	4.01	3.99	3.87	3.20	3.87	4.09	4.13	3.60	3.85	4.00	
Expt. 3	3	2	3.88	4.12	4.12	4.11	4.09	4.07	3.98	3.74	4.07	4.09	4.07	3.93	4.06	4.12	
Expt. 4	3	2	3.96	4.19	4.19	4.18	4.18	4.16	4.07	3.88	4.18	4.16	4.17	4.06	4.13	4.17	
Expt. 5	1	2	2.38	2.50	2.50	2.50	2.49	2.48	2.40	2.27	2.46	2.50	2.57	2.46	2.50	2.50	
Expt. 6	2	2	3.26	3.36	3.35	3.35	3.34	3.32	3.23	3.12	3.32	3.29	3.30	3.28	3.32	3.35	
Expt. 7	3	2	3.94	4.07	4.06	4.06	4.05	4.03	3.89	3.50	3.99	4.07	4.05	3.85	3.96	4.05	
Expt. 8	4	2	4.80	4.65	4.65	4.64	4.64	4.60	4.48	3.72	4.51	4.72	4.77	4.15	4.44	4.61	
Expt. 9	3	1	3.30	3.14	3.13	3.13	3.12	3.10	3.05	2.90	3.09	3.14	3.18	3.08	3.12	3.13	
Expt. 10	3	1.5	3.78	3.64	3.63	3.63	3.62	3.60	3.52	3.41	3.62	3.63	3.60	3.58	3.61	3.62	
Expt. 11	3	2	3.97	3.92	3.92	3.92	3.91	3.89	3.78	3.45	3.86	3.94	3.95	3.70	3.83	3.92	
Expt. 12	3	3	4.04	4.08	4.09	4.08	4.07	4.05	3.95	3.55	4.01	4.10	4.13	3.74	3.94	4.07	
Expt. 13	3	4	4.11	4.26	4.26	4.26	4.23	4.22	4.12	3.69	4.17	4.27	4.28	3.69	4.03	4.24	
Expt. 14	2	2	2.52	2.80	2.80	2.80	2.77	2.76	2.66	2.52	2.76	2.78	2.76	2.72	2.77	2.79	
Expt. 15	3	2	4.01	4.01	4.02	4.03	4.04	4.01	3.95	3.09	3.73	4.13	4.09	3.57	3.86	4.02	
Expt. 16	4	2	5.44	5.20	5.20	5.20	5.19	5.16	5.06	3.93	4.94	5.28	5.33	4.68	4.93	5.19	
Expt. 17	2	2	2.64	2.65	2.65	2.64	2.63	2.62	2.55	2.41	2.59	2.62	2.61	2.55	2.60	2.63	
Expt. 18	3	2	3.99	4.10	4.10	4.09	4.08	4.06	3.95	3.49	4.01	4.11	4.12	3.84	3.99	4.08	
Expt. 19	4	2	5.36	5.45	5.45	5.44	5.43	5.41	5.26	4.35	5.25	5.48	5.53	5.07	5.28	5.42	

TABLE II. Regression analysis of the results of the *in vitro* flow phantom experiment.

Parameters	Goodness of fit R^2	Slope	Slope standard error	95% CI slope	Intercept	Intercept standard error	95% CI intercept
$L = 30$ mm, no noise							
Frame rate (Hz)							
150	0.951	0.922	0.051	[0.815, 1.029]	0.316	0.199	[-0.106, 0.737]
75	0.951	0.923	0.051	[0.816, 1.030]	0.31	0.201	[-0.114, 0.734]
50	0.951	0.921	0.051	[0.814, 1.029]	0.312	0.201	[-0.605, 0.342]
30	0.95	0.924	0.051	[0.815, 1.033]	0.294	0.203	[-0.139, 0.719]
25	0.95	0.918	0.051	[0.809, 1.027]	0.294	0.203	[-0.135, 0.723]
15	0.947	0.901	0.051	[0.792, 1.010]	0.26	0.203	[-0.169, 0.690]
$fr = 50$ Hz, no noise							
Segment length (mm)							
10	0.689	0.579	0.094	[0.38, 0.778]	1.059	0.373	[0.272, 1.846]
20	0.924	0.858	0.06	[0.732, 0.984]	0.46	0.236	[-0.038, 0.958]
30	0.951	0.924	0.051	[0.815, 1.033]	0.294	0.203	[-0.139, 0.719]
40	0.963	0.955	0.045	[0.960, 1.050]	0.205	0.178	[-0.171, 0.581]
50	0.969	0.966	0.042	[0.876, 1.055]	0.178	0.166	[-0.171, 0.528]
$L = 30$ mm, $fr = 50$ Hz							
SNR (dB)							
6	0.854	0.754	0.076	[0.599, 1.321]	0.69	0.299	[0.060, 1.321]
10	0.916	0.841	0.0618	[0.711, 0.972]	0.508	0.244	[-0.007, 1.024]
20	0.95	0.926	0.051	[0.809, 1.024]	0.323	0.201	[-0.102, 0.747]

Figure 9 displays the regression slopes as function of the frame rate for a fixed vessel length of 30 mm [Fig. 9(a)], and the regression slopes as function of the vessel segment length for a frame rate of 50 Hz [Fig. 9(b)]. Figure 10 shows the gold standard wave measured by the flow meter, and the respective curves delivered by our method using different x-ray frame rates.

The data measured on the cerebral vessel phantom are presented in Table III. The data are graphically represented in Fig. 11.

III.B. Internal carotid artery

Here we report on some preliminary results of the ongoing clinical study. Figure 12 displays x-ray internal carotid artery

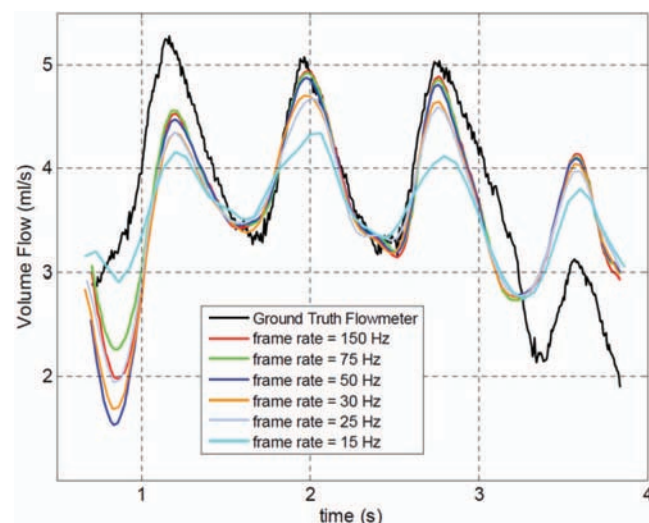


FIG. 10. Flow curves measured with decreasing frame rates.

flow curves in the case of three exemplary patients (Fig. 13), obtained with different injection conditions. They are compared to Doppler volume flow data, which is plotted in the same graph. The various acquisitions per patient were obtained consecutively, and the data were shifted to match the cardiac phase of the curves. For each patient the average arterial flow per acquisition is reported.

TABLE III. Experimental conditions and flow estimations during *in vitro* experiments on the vessel phantom.

	View	Pump		Frequency (Hz)	Injection (ml/s)	Flow	
		Pump (ml/s)	pulsatility (%)			meter (ml/s)	X-ray (ml/s)
Expt. 21	1	4	40	1	3	8.02	8.31
Expt. 22	1	4	40	1.3	3	8.00	8.27
Expt. 23	1	4	70	1	2	6.60	6.89
Expt. 24	1	4	70	1	1.5	5.96	6.45
Expt. 25	1	4	70	1.3	1.5	6.07	6.21
Expt. 26	1	3	100	1	3	6.99	6.70
Expt. 27	1	3	70	1.3	2	5.64	5.72
Expt. 28	1	3	70	1	2	5.51	5.26
Expt. 29	1	3	70	1.3	1	3.97	3.88
Expt. 30	1	2	70	1	1	2.90	2.96
Expt. 31	1	2	70	1	2	4.94	4.80
Expt. 32	1	2	70	1.3	2	4.96	4.61
Expt. 33	1	2	40	1	1	2.90	2.69
Expt. 34	1	1	70	1	1.5	3.12	3.06
Expt. 35	2	4	70	1.3	2	6.78	7.14
Expt. 36	2	3	40	1.3	2	5.89	6.01
Expt. 37	2	3	70	1	2	5.82	5.84
Expt. 38	2	3	70	1.3	1	3.99	4.23
Expt. 39	2	2	40	1.3	1	3.09	3.03
Expt. 40	2	1	70	1	2	3.71	3.85
Expt. 41	2	1	70	1	1	2.11	2.12

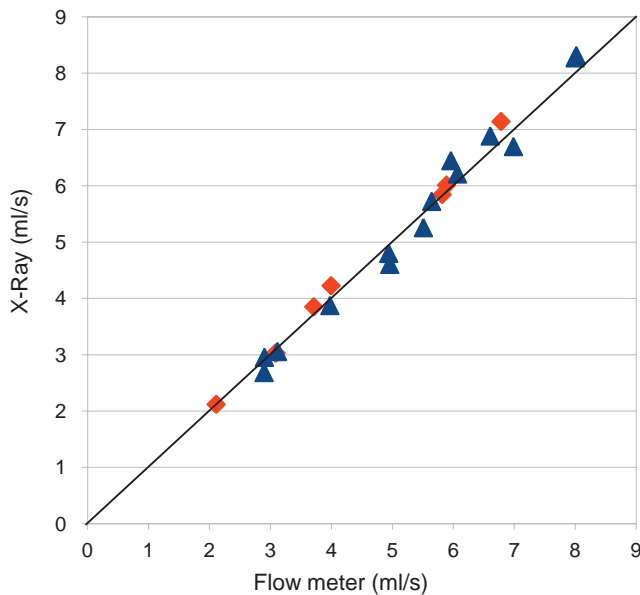


FIG. 11. Gold standard delivered by the flow meter (x-axis) versus the flow measurements using the proposed method (y-axis). Triangles represent the measurements from view 1 and the diamonds the measurements from view 2. The diagonal line indicates the ideal match.

Concerning the first patient acquisitions, we used low injection rates (1.5 cc/s, 2 cc/s, 3 cc/s) in order to stay close to the physiologic conditions. The carotid artery flow curves displaying the temporal variation of the physiologic flow are comparable to Doppler records for patients 1 and 2. For patient 3 the Doppler ultrasound measured arterial flow is considerably higher than reported by the x-ray measurements. The x-ray acquisition parameters and the related dose is reported in Table IV.

IV. DISCUSSION

From the phantom experiment results in Tables I and II it can be concluded that the length of the segment used for measurements should be $L \geq 20$ mm in order to obtain a good flow estimation. This implies that an almost straight segment of 20 mm should be present in the target vessel, which may not be the case for very curved vessels. However, there are many arteries where a measurable location can be found, such as the petrous segment, the intracranial carotid, and the intracranial vessels at the level of the Willis polygon sections, etc. An added noise of 20 dB in SNR compared to the original data does not produce any significant performance degradations. For $L = 30$ mm, all frame rates between 150 and 50 Hz performed at a comparable level, but results were worse for $fr < 50$ Hz. Within this range, the regression slope analysis gives a standard error in the order of 0.05, with a 95% CI comprising the ideal ratio 1. This is a clear indicator for the validity of the method. The intercept estimations exhibit a confidence interval comprising the null hypothesis.

Since the underlying principle of the used algorithm is based on following the contrast modulation, the x-ray acquisition parameters hardly influence the algorithm, as long as

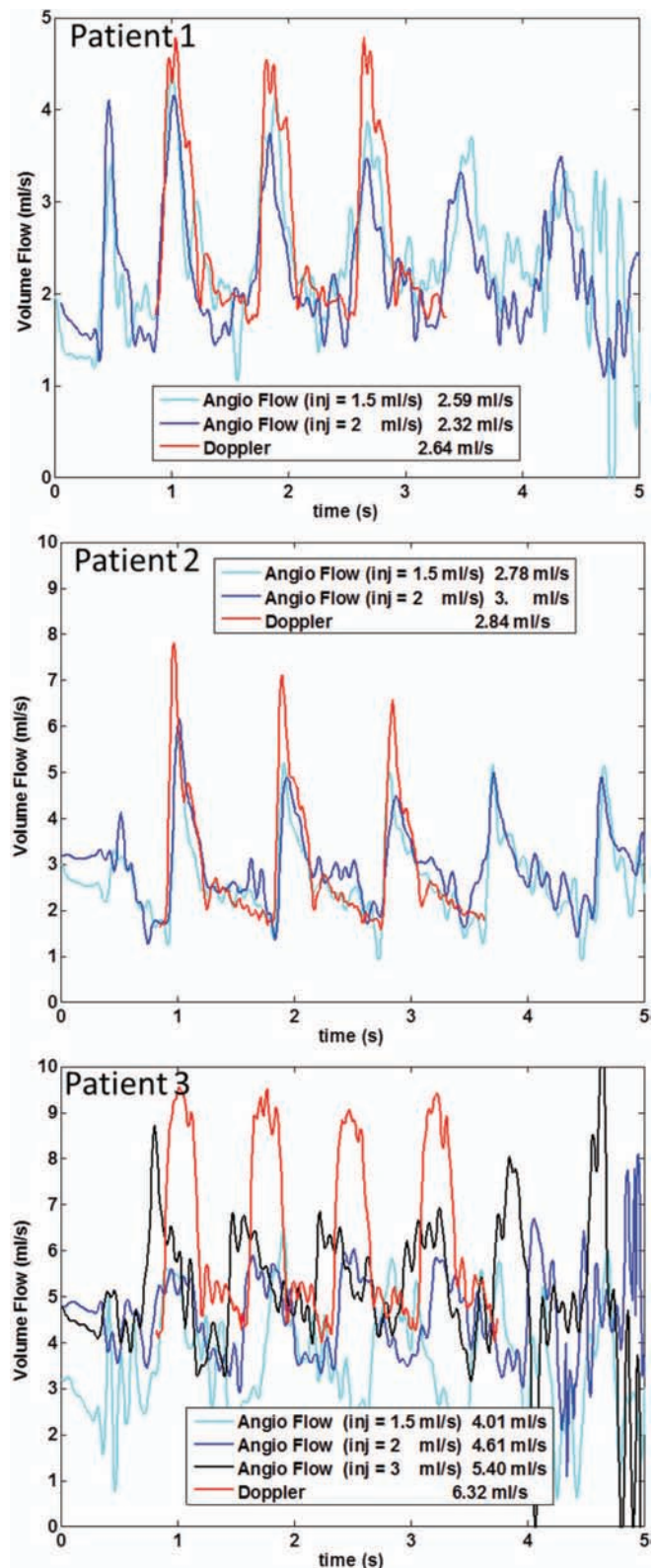


FIG. 12. X-ray and Doppler flow curves for three exemplary patient cases. For each line the average arterial flow is reported.

the signal to noise ratio is not impacted too much. After all, the algorithm tracks the phase of the contrast wave, which is not impacted by the amplitude. The algorithm assumes that the displacement of the cardiac pressure through the vessel

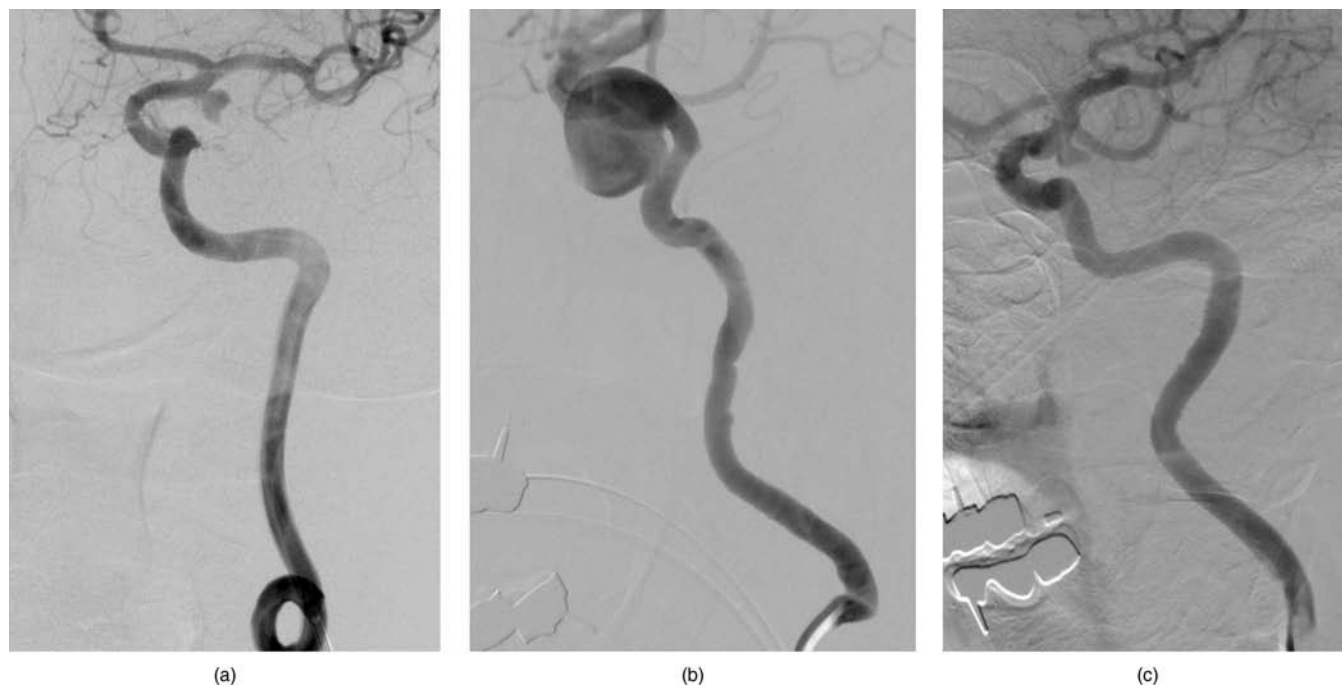


FIG. 13. DSA acquisitions of the three presented patients. Left: patient 1, middle: patient 2, right: patient 3.

corresponds with the overall blood flow speed, which is a simplification of the different velocities that can be found radially within the vessel.^{19,20} It should be taken into account that the presence of a catheter in the artery and the injection of contrast medium modifies the physiological blood flow. According to Mulder *et al.* the physiological flow is increased by approximately 20% of the injection rate, due to the resistance of the vascular system.²¹ This would imply an increase of 0.2 to 0.8 ml/s of the flow, depending on the injection protocol. It should be noted that the described approach cannot quantify secondary or laminar flow patterns. Also the distance from the injection site to the measuring area should be sufficiently large (at least ten artery diameters according to Lieber *et al.*¹⁷), in order to achieve a good mix of the blood and the contrast agent. In order to obtain reliable measurements it is advised to use contrast injection rates that are lower than the arterial flow. The x-ray dose of the flow acquisition was comparable to that of a regular angiogram, see Table IV. Earlier attempts to use optical flow algorithms could only detect relative modest velocities.⁷ This limitation is lifted by applying the warping operation described in Sec. II.A and by using

modern x-ray C-arm equipment, since the frame rate of the acquisition can be substantially higher than in the past.

Based on the phantom experiments, we expect that even small region of interests on vessel segment lengths of $L \geq 20$ mm can be used for measuring flow with the described approach. One limitation of the *in vitro* setup is the fact that it does not provide a pressure/resistance driven system, as is the case in the real vascular system. Furthermore, it possessed only very minimal secondary flow effects. From the *in vitro* results, we conclude that a frame rate higher than 50 Hz allows measuring flows in the range of 2 ml/s to 6 ml/s with an accuracy of 5%. Overall, it can be said that the proposed technique can be used in routine conditions with standard acquisition protocols.

When considering the comparison of the patient measurements, it should be taken into account that Doppler ultrasound measurements may suffer from effects such as non optimal beam-vessel angle definition and/or spectral broadening.^{22–24} Transcranial Doppler ultrasound (TCD) has been described as a non-invasive imaging technique in neurological procedures.²⁵ The proposed x-ray based method

TABLE IV. X-ray acquisition parameters and associated dose measurements for a patient case.

	DAP (mGy cm ²)	cm	mGy/s	nGy/frame	kV	mA s	Frames/s	Images	FOV (cm)	DFI	Position
Standard	10 172	22	2.00	33	80	48	2	21	31	120	Lateral
Standard	19 430	22	4.72	79	85	109	2	17	31	114	AP
3DRA	31 550	22	16.30	272	97	263	30	120	31	120	Rotational
Flow	8907	16	4.21	70	71	628	60	496	22	120	Oblique
Flow	9386	16	4.18	70	71	624	60	526	22	120	Oblique
Flow	9016	16	4.25	71	71	630	60	497	22	120	Oblique

for flow assessment can be used at locations that cannot be reached by Doppler ultrasound, such as the intra petrous or intracranial carotid segments.

The described technique may be, e.g., applied in the context of the treatment of vasospasms or intracranial stenoses that ought to be evaluated during or just after angioplasty. It can also be applied to evaluate the recently introduced flow diverting stents (FDS),^{26–28} used to treat intra-cranial aneurysms. These devices have a dense porosity that is capable of modifying the intra-aneurysmal blood flows, inducing progressive thrombosis and vascular remodeling. The motion of the contrast wave can be observed and quantified within the aneurysm sac, using an adequate 2D optical flow method. While such a measurement is difficult to relate to an absolute quantification of the flow inside the aneurysm due to the volumetric nature of the flow patterns within the aneurysm, it is possible to compare the apparent motion measured just before and after the FDS placement, using the same projection views. Aneurysm diagnosis and treatment with FDS can benefit greatly from peri-interventionally measuring the blood flow characteristics prior and after the stent has been placed, to evaluate whether another FDS is needed.²⁹ Such a technique is an added value that would improve the functional capability of DSA imaging modality in endovascular procedures.

V. CONCLUSION

In this paper, we proposed and evaluated an approach to estimate the arterial blood flow from DSA sequences. The results obtained on experimental data demonstrated the validity of this approach. Preliminary tests operated on several clinical cases give good confidence on its feasibility during interventional procedures. A substantial clinical evaluation of this technique is on the way to assess its accuracy.

The proposed x-ray based method for flow assessment is particularly useful for perioperative applications where intracranial Doppler ultrasound cannot be reliably or routinely used. This is particularly useful in the context of flow diverting stents (FDS), targeted at intra-cranial aneurysm treatment. In this procedure the quantification of the blood flow prior to and after stent deployment can aid in evaluating the efficacy of the FDS.

Current and future work comprises a comprehensive clinical validation with respect to Doppler ultrasound, and the correlation of x-ray based flow measurements to the clinical outcome of aneurysm treatment by flow diverter placement. In these studies, the impact of the presence of the catheter in the artery and the contrast injection on the physiological flow will be further studied. Furthermore, it can be investigated how the presented technique can be applied to curved vessels.

^{a)} Author to whom correspondence should be addressed. Electronic mail: danny.ruijters@philips.com

¹L. Augsburger, P. Reymond, E. Fonck, Z. Kulcsar, M. Farhat, M. Ohta, N. Stergiopoulos, and D. A. Rüfenacht, "Methodologies to assess blood flow in cerebral aneurysms: Current state of research and perspectives," *J. Neuro-radiol.* **36**, 270–277 (2009).

- ²D. M. Sforza, C. M. Putman, and J. R. Cebra, "Hemodynamics of cerebral aneurysms," *Annu. Rev. Fluid Mech.* **41**, 91–107 (2009).
- ³N. U. Ko, A. S. Achrol, M. Chopra, M. Saha, D. Gupta, W. S. Smith, R. T. Higashida, and W. L. Young, "Cerebral blood flow changes after endovascular treatment of cerebrovascular stenoses," *AJNR Am. J. Neuro-radiol.* **26**, 538–542 (2005).
- ⁴C. M. Quick, T. Hashimoto, and W. L. Young, "Lack of flow regulation may explain the development of arteriovenous malformations," *Neurol. Res.* **23**, 641–644 (2001).
- ⁵Q. Sun, A. Groth, M. Bertram, I. Waechter, T. Bruijns, R. Hermans, and T. Aach, "Phantom-based experimental validation of computational fluid dynamics simulations on cerebral aneurysms," *Med. Phys.* **37**, 5054–5065 (2010).
- ⁶A. Groth, I. Waechter-Stehle, O. Brina, F. Perren, V. Mendes-Pereira, D. Rüfenacht, T. Bruijns, M. Bertram, and J. Weese, "Clinical study of model-based flow quantification on cerebrovascular data," *Proc. SPIE* **7964**, 79640X (2011).
- ⁷S. D. Shpilfoygel, R. A. Close, D. J. Valentino, and G. R. Duckwiler, "X-ray videodensitometric methods for blood flow and velocity measurement: A critical review of literature," *Med. Phys.* **27**, 2008–2023 (2000).
- ⁸L. Sarry, Y. J. Peng, and J. Y. Boire, "Blood flow velocity estimation from x-ray densitometric data: An efficient numerical scheme for the inverse advection problem," *Phys. Med. Biol.* **47**, 149–162 (2002).
- ⁹H. Bogunović and S. Lončarić, "Blood flow and velocity estimation based on vessel transit time by combining 2D and 3D X-ray angiography," in *MICCAI'06 Proceedings of the 9th International Conference on Medical Image Computing and Computer-Assisted Intervention* (Springer-Verlag Berlin, Heidelberg, 2006), Vol. 9 (Pt. 2), pp. 117–124.
- ¹⁰K. S. Rhode, T. Lambrou, D. J. Hawkes, and A. M. Seifalian, "Novel approaches to the measurement of arterial blood flow from dynamic digital x-ray images," *IEEE Trans. Med. Imaging* **24**, 500–513 (2005).
- ¹¹I. Waechter, J. Bredno, J. Weese, D. C. Barratt, and D. J. Hawkes, "Using flow information to support 3D vessel reconstruction from rotational angiography," *Med. Phys.* **35**, 3302–3316 (2008).
- ¹²L. Sarry, J.-Y. Boire, M. Zanca, J.-R. Lussion, and J. Cassagnes, "Assessment of stenosis severity using a novel method to estimate spatial and temporal variations of blood flow velocity in biplane coronarography," *Phys. Med. Biol.* **42**, 1549–1564 (1997).
- ¹³R. P. Wildes, M. J. Amabile, A.-M. Lanzillotto, and T.-S. Leu, "Recovering estimates of fluid flow from image sequence data," *Comput. Vis. Image Underst.* **80**, 246–266 (2000).
- ¹⁴B. D. Lucas and T. Kanade, "An iterative image registration technique with an application to stereo vision," in *Proceedings of Imaging Understanding Workshop* (DARPA, New Orleans, LA, 1981), pp. 121–130.
- ¹⁵S. Baker and I. Matthews, "Lucas-Kanade 20 years on: A unifying framework," *Int. J. Comput. Vis.* **56**, 221–255 (2004).
- ¹⁶D. Ruprecht and H. Müller, "Image warping with scattered data interpolation," *IEEE Comput. Graphics Appl.* **15**, 37–43 (1995).
- ¹⁷B. B. Lieber, C. Sadasivan, Q. Hao, J. Seong, and L. Cesar, "The mixability of angiographic contrast with arterial blood," *Med. Phys.* **36**, 5064–5078 (2009).
- ¹⁸J. R. Womersley, "Method for the calculation of velocity, rate of flow and viscous drag in arteries when the pressure gradient is known," *J. Physiol.* **127**, 553–563 (1955).
- ¹⁹G. Taylor, "Dispersion of soluble matter in solvent flowing slowly through a tube," *Proc. R. Soc. London, Ser. A* **219**, 186–203 (1953).
- ²⁰G. Taylor, "The dispersion of matter in turbulent flow through a pipe," *Proc. R. Soc. London, Ser. A* **223**, 446–468 (1954).
- ²¹G. Mulder, A. C. B. Bogaerds, P. Rongen, and F. N. van de Vosse, "The influence of contrast agent injection on physiological flow in the circle of Willis," *Med. Eng. Phys.* **33**, 195–203 (2011).
- ²²P. N. Burns, "Measuring volume flow with doppler ultrasound—an old nut," *Ultrasound Obstet. Gynecol.* **2**, 238–241 (1992).
- ²³P. R. Hoskins, "Estimation of blood velocity, volumetric flow and wall shear rate using Doppler ultrasound," *Ultrasound* **19**, 120–129 (2011).
- ²⁴C. K. Holland, M. J. C. Kenneth, J. Taylor, J. L. Alderman, K. Purushothaman, and T. R. McCauley, "Volumetric flow estimation *in vivo* and *in vitro* using pulsed-Doppler ultrasound," *Ultrasound Med. Biol.* **22**, 591–603 (1996).
- ²⁵S.-A. Ahmadi, M. Baust, A. Karamalis, A. Plate, K. Boetzel, T. Klein, and N. Navab, "Midbrain segmentation in transcranial 3D ultrasound for

- parkinson diagnosis,” in *International Conference on Medical Image Computing and Computer Assisted Intervention (MICCAI)* (Springer-Verlag, Berlin, Heidelberg, 2011), pp. 18–22.
- ²⁶E. Crobbedu, G. Lanzino, D. F. Kallmes, and H. J. Cloft, “Marked decrease in coil and stent utilization following introduction of flow diversion technology,” *J. NeuroInterv. Surg.*, (2012), epub ahead of print.
- ²⁷X. Armoiry, M. Paysant, D. Hartmann, G. Aulagner, and F. Turjman, “Interest of flow diversion prostheses in the management of unruptured intracranial aneurysms,” *Int. J. Vasc. Med.* **2012**, 654627 (2012).
- ²⁸J. Berge, A. Biondi, P. Machi, H. Brunel, L. Pierot, J. Gabrillargues, K. Kadziolka, X. Barreau, V. Dousset, and A. Bonafé, “Flow-diverter silk stent for the treatment of intracranial aneurysms: 1-year follow-up in a multicenter study,” *AJNR Am. J. Neuroradiol.* **33**, 1150–1155 (2012).
- ²⁹V. Mendes Pereira, O. Bonnefous, R. Ouared, O. Brina, J. Stawiaski, H. Aerts, D. Ruijters, A. P. Narata, P. Bijlenga, K. Schaller, and K.-O. Lovblad, “A DSA-based method using contrast motion estimation for the assessment of the intra-aneurysmal flow changes induced by flow diverter stents,” *AJNR Am. J. Neuroradiol.* (in press).